Check for
updates

Negative Magnetoresistance Behavior in Polymer Spin Valves Based on Donor–Acceptor Conjugated Molecules

Naihang Zheng, Xiang Wang, Yuanhui Zheng, Dong Li, Zuzhang Lin, Weifeng Zhang, Kui-juan Jin,* and Gui Yu*

Organic spin valves (OSVs) have become an essential building block of next-generation memory devices which focus on spin degree of transporting carriers. Meanwhile, negative magnetoresistance (MR) effect in the OSV devices is increasingly observed which deserves further exploration for the rich spin physics behind. In this work, the negative MR response in ferromagnetic (FM) metal-based OSVs using donor–acceptor (D–A) conjugated polymer based on the naphthalenediimide units as a spacer material is observed. The negative MR effect does not result from negative polarization at spin injection and detection interface as well as tunneling anisotropic magnetoresistance effect, but from the spin transport inside the D–A polymer spacer. Even the stacking sequence of the spin injection and detection electrodes is reversed or changed the polymer coating solvents, the D–A polymer contributed negative MR response still can be observed. For further identifying negative MR origin, the bottom FM metal polarizer is replaced into high-polarization $La_{0.7}Sr_{0.3}MnO_3$ thin film, negative MR feature is well reproduced. Based on these points, it is deduced that the spin-orientation reversal inside D–A polymer spacer is the ultimate reason for such negative MR response. The filtering-like spin reversal activity is also in positive proportion to intermolecular interaction.

1. Introduction

Organic spin valves (OSV) is a pivotal ingredient of next-generation spin-memory devices which aim to exploit advantageous long spin lifetime of organic semiconductors.[1–6] Three basic characteristics are required for constructing the OSV

devices, namely ferromagnetic (FM) spin injectors and detectors and non-ferromagnetic organic medium. When evaluating OSV device performance, magnetoresistance (MR) behavior is an important criterion.[7–11] Undoubtedly, decent MR value is strongly expected for its close proof to long distance spin-conserved transport. Continuous efforts of seeking suitable spin polarizer and transport media fueled the development of OSVs during the past decade.[2–4,11–14] On the other hand, debate on MR signal has never ceased since the first report on organic giant magnetoresistance by Xiong.[7] In general, MR response in a prototype OSV device is considered to be positive, namely device resistance under magnetization antiparallel states is larger than that of parallel states. However, negative (abnormal) MR response in OSVs is increasingly discovered thus must not be fortuity. Consequently, distinguishing the working mechanisms of the negative MR signals becomes an important component of organic spintronics. To date, there are several viewpoints to explain this abnormal spin response: 1) Negative polarization is the most representative also the earliest explanation which is primarily extracted from Julliere tunneling formula.[15–17] That is when spin injector is positively (negatively) polarized, while spin detector is negatively (positively) polarized, the MR behavior is negative. However, such explanation is invalid when injecting

N. H. Zheng, Dr. Y. H. Zheng, D. Li, Z. Z. Lin,
Dr. W. F. Zhang, Prof. G. Yu
Beijing National Laboratory for Molecular Sciences
CAS Research/Education Center for Excellence in Molecular Sciences
Institute of Chemistry
Chinese Academy of Sciences
Beijing 100190, P. R. China
E-mail: yugui@iccas.ac.cn
N. H. Zheng, D. Li, Prof. G. Yu
School of Chemical Sciences
University of Chinese Academy of Sciences
Beijing 100049, P. R. China

X. Wang, Prof. K. J. Jin
Beijing National Laboratory for Condensed Matter Physics
Institute of Physics
Chinese Academy of Sciences
Beijing 100190, P. R. China
E-mail: kjjin@iphy.ac.cn
X. Wang, Prof. K. J. Jin
Songshan Lake Materials Laboratory Dongguan
Guangdong 523808, P. R. China
X. Wang, Prof. K. J. Jin
School of Physical Sciences
University of Chinese Academy of Sciences
Beijing 100049, P. R. China

**ADVANCED
SCIENCE NEWS**
www.advancedsciencenews.com

**ADVANCED
MATERIALS
INTERFACES**
www.advmatinterfaces.de

and detecting interfaces share the same polarized direction. Besides, mechanically using this concept can possibly leave out key information from molecular transport media. 2) Recently, spinterface issue aroused worldwide attention in spintronics field due to the underlying rich spin physics. This phenomenon was also used for explaining negative OSV effect.[18–20] Filtering interfacial hybrid state is the core of this concept which can reverse original spin orientation of polarized carriers and thus leads to negative MR response.[20–22] Though such hybridization can sometimes improve spin injection efficiency and trigger more novel spin discoveries, we should not forget the primitive goal of OSV is achieving long distance spin-preserved transport in organic spacer rather than undertaking interface engineering. 3) During the entire fabrication process of vertical OSVs, top metal depositing process should be paid extra attention due to its possible damage on soft organic layers. Beyond that, such unexpected metal/organic interpenetration can sometimes induce negative MR response which is also defined as "filaments effect."[23–26] Once that happens, it becomes harsh to analyze how organic spacer influences device spin transport performance. 4) Ferroelectric materials have been regarded as an important molecular platform to manipulate spin polarization by electrical means.[27] OSVs exploiting such kind of materials have also been probed thoroughly during recent years. One featuring characteristics of such device is the corresponding MR signal can be reversed when converting test electric field polarity.[28–31] In this case, negative MR response relies on dipole activity inside ferroelectric media. 5) To reinforce electrical or photovoltaic performance of organic semiconductors, molecular doping is one efficient strategy which has been extensively used.[32,33] Such method also works significantly on tuning spin transport performance of OSVs, for recent examples of negative OSV signals.[34–37] The above five negative MR resources have made great contribution to better understanding of spin dynamics inside organics and OSV working principle. However, these explanations were mainly aimed at small molecules and oligomers. Understanding the origin of the negative MR signals observed in other materials, such as recently hot-discussing donor–acceptor (D–A) conjugated polymers, is still in lack.

In recent years, D–A conjugated polymers have caught increasing eyeballs for their limitless building blocks option and strong intermolecular interactions. Resulting huge success in organic field effect transistor (OFETs) and organic solar cells further demonstrated their potential in next-generation electrical functional devices.[38–41] At the same time, spin transport performance of the D–A conjugated polymers was also under investigation and recently, acquired some inspiring results.[11,42–46] Nevertheless, the in-depth understanding of spin transport performance of the D–A semiconducting polymer is inadequate. There are two methods to unlock such dilemma. One protocol is integrating spin transport study intensively with polymer thin film growing conditions.[45] The other is utilizing structure engineering project when discussing microscopic spin dynamics inside the D–A conjugated molecules.[44,46]

Herein, we selected a D–A naphthalenediimide (NDI)-based conjugated polymer PNVT-CN-8 containing 2,3-bis(thiophen-2-yl)acrylonitrile units as a nonferromagnetic interlayer to fabricate OSV devices and surprisingly found the polymer

can solely induce negative MR response. FM metals were used for OSV construction affording NiFe/Au/D–A polymer/Co/Au stacking in vertical configuration. Resulting negative OSV signal was rather stable even after 30 days air-exposure and did not encounter dramatic change on MR shape against varying current. Such intriguing spin response had nothing to do with interfacial negative polarization or tunneling anisotropic magnetoresistance (TAMR) effect. Even we reversed the spin injector (NiFe)/detector (Co) sequence and made an alternation on polymer dissolving solvents, the negative MR phenomenon was still observed. For deeper insights of the negative MR resource, we replaced bottom NiFe spin injector with high-polarization $La_{0.7}Sr_{0.3}MnO_3$ (LSMO) electrode, and added another layer of polymethylmethacrylate (PMMA) at top interface. Amazingly, the negative MR characteristics were retained once this NDI-based polymer participated into OSV construction. Based on these results, we argued that the measured negative MR response was governed by spin dynamics inside the NDI-based polymer. Spin orientation of polarized carriers might be reversed when travelling through such solution-processed D–A polymer thin film, similar to the spin-filtering phenomenon discovered before. These findings unveiled another role of solution-processed D–A polymers on spin information processing, namely manipulating spins by polymer conjugated backbones.

2. Results and Discussion

Chemical structure of interlayer polymers used in the OSV devices is depicted in **Figure 1**a. This vinyl-bridge D–A conjugated polymer is named as PNVT-CN-8 which showed ambipolar charge transport behavior and good spin transport performance as we studied before.[46–48] Moreover, PNVT-CN-8 also has good solubility in different solvents, hence offers a good platform to study solvent effect on its spin transport performance.[47] To guarantee successful OSV operation, the device with a configuration structure of NiFe (bottom, 12 nm)/Au (3 nm)/PNVT-CN-8 (25 nm)/Co (top, 12 nm)/Au (25 nm) was fabricated as shown in Figure 1b. The 3 nm Au is a protective metallic barrier to solve ferromagnet contamination during solution procedure of the polymer thin film, with another task of injecting polarized carriers.[3,49–51] Usually, the ultra-thin AlOx buffer layer is a very good option in fabrication of organic spin valves. Explicitly speaking, there are leaky and non-leaky AlOx protective layers.[52] The leaky AlOx is more advantageous on identifying molecular MR contribution because its metal-like conducting behavior cannot enlarge junction resistance too fiercely. However, using the AlOx protective layer is not perfect because of its inevitable introduction of oxygen. Recently, Riminucci et al. discovered employing AlOx layer could bring into oxygen impurities thus resulting in negative MR behavior.[35,36] For our OSV devices based on the NiFe bottom electrodes, the oxygen introduced during the preparation of AlOx layer could oxidize the NiFe electrodes during spin-coating process of neighboring polymer thin films. So, we did not choose the ultra-thin AlOx as the protective layer to fabricate the OSV devices. Instead, we choose gold as the protective layer due
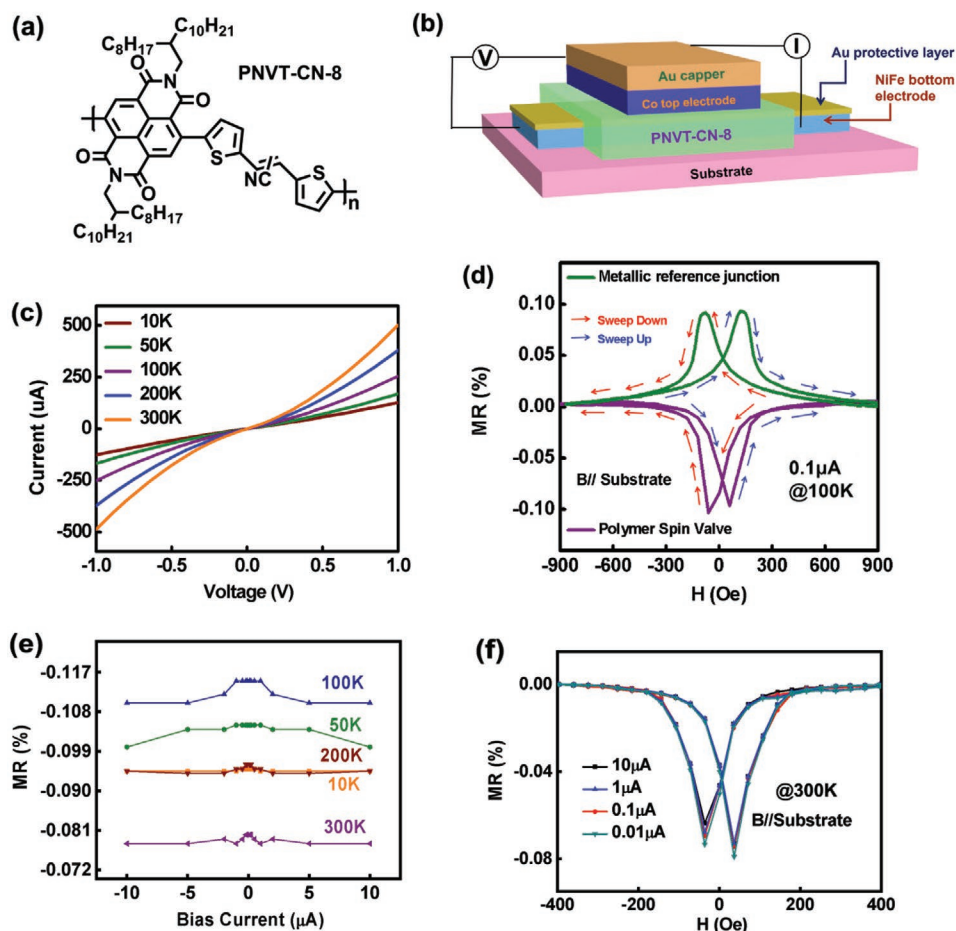
**ADVANCED
SCIENCE NEWS**

www.advancedsciencenews.com

**ADVANCED
MATERIALS
INTERFACES**

www.advmatinterfaces.de

Figure 1. The OSV device with the configuration structure of the NiFe (12 nm)/Au (3 nm)/PNVT-CN-8 (25 nm)/Co (12 nm)/Au (25 nm). a) Molecular structures of the conjugated polymer PNVT-CN-8. b) Device structure of the OSVs based on PNVT-CN-8. c) Current–voltage characteristics of the OSV devices based on PNVT-CN-8 measured at different temperatures. d) MR loops of all metal devices with configuration structure of the NiFe (12 nm)/Au (3 nm)/Co (12 nm)/Au (25 nm) and the OSV devices based on PNVT-CN-8 measured at 100 K. e) Current dependence of the MR ratios for the OSV devices based on PNVT-CN-8 measured at different temperatures. f) MR loops of the OSV devices based on PNVT-CN-8 measured under different currents at 300 K.

to its following advantages: 1) Work function of Au is close to the HOMO energy level of our polymer PNVT-CN-8, which is favorable for spin-polarized carrier injection.[46,47] 2) The preparation stage of Au layer did not damage the ferromagnetism of bottom NiFe electrode because Au was in-situ deposited onto the surface of the NiFe electrode without breaking the vacuum. The 25 nm polymeric spacer was spin coated directly onto the Au-capped NiFe stripes using 1,2-dichlorobenzene (DCB) solution. Thermal treatment was performed subsequently (120 °C, 30 min) before depositing top FM metals. The HOMO/LUMO energy levels of PNVT-CN-8 match well with the work functions of neighboring metals, hence offer a good premise to spin polarized injection.[46,47] Before discussing MR behavior of the OSV based on PNVT-CN-8, corresponding charge transport properties were examined first. Four-probe testing mode was employed for current–voltage (I–V) characterization as shown in Figure 1c, which exhibits good symmetry and evident non-linearity. This is a good indicative of balanced ambipolar spin injection at two metal/polymer interfaces, also a solid

proof about polymer's contribution to device resistance. Since the device resistance increases with elevating temperature, we argue that massive short-circuiting did not occur during top metal deposition. Additionally, these electrical responses are rather stable against continuous back and forth sweeping (under fixed voltage) over one hundred times (Figure S1, Supporting Information). Hence we believe that the following MR measurement results are not interrupted by metal filaments.[52]

As usual, external in-plane magnetic field was applied parallel to these metal/organic hybrid junctions under constant current DC mode. The angle of the in-plane magnetic field relative to the easy axis of counter FM electrodes was set into 45°. MR ratio was calculated by formula defined as $MR = (R_{AP} - R_p)/R_p \times 100\%$, where R_{AP} and R_p refer to resistance measured under antiparallel and parallel states, respectively. The OSV device with a configuration structure of NiFe (bottom,12 nm)/Au (3 nm)/PNVT-CN-8 (25 nm)/Co (top, 12 nm)/Au (25 nm) displayed evident negative MR response as depicted in Figure 1d, which is opposite to situation of robust

positive MR response measured in metallic background structure of NiFe (bottom)/Au (3 nm)/Co (top)/Au. MR trace of this negative spin response was very smooth with no fierce signal/noise fluctuation. In addition, such negative OSV signal does not vanish monotonously with increasing temperature unlike all-metal reference junction NiFe (bottom, 12 nm)/Au (3 nm)/Co (top, 12 nm)/Au (25 nm) (Figure S2, Supporting Information). There are two main reasons accounting for such nonmonotonous temperature dependence: 1) Compared to the all-metal reference structure, additive spin-polarized carriers are injected through the molecular frontier levels near the metal/organic interfaces. This is also another solid proof of polymer's contribution to entire negative OSV signal.[50] 2) We notice the MR ratios in the polymer-contained spin valve first increases and then drops with the increasing temperature. Such phenomenon is not incomprehensible since the travelling distance for polarized carriers in non-ferromagnetic media has exceed the tunneling limit.[53] In this case, spin dephasing induced by phonon scattering under high temperature cannot be neglected and that is why the MR ratios from 100 to 300 K decreases with elevation on temperature.[54] Furthermore, we found this negative MR effect can persist up to 300 K. Corresponding MR curves are shown in Figure S3a, Supporting Information, whose switching region matches well with counter spin polarizer coercive values (Figure S3b, Supporting Information). Before discussing the negative MR origin, we checked whether such negative MR response was just coincidence. Our experiments showed that this negative MR effect could not only be repeated, but also exhibited good air-stability near to 30 days (Figure S4, Supporting Information). This powerfully demonstrated our negative OSV effect is definitely not an accidental result. As constantly emphasized in past OSV-related researches, bias electrics had a huge influence on the MR behavior.[23,55] Wu discovered reversing bias polarity and changing current size led to MR reversal.[55] Vinzelberg also discovered tuning external electric field dramatically transformed shape of measured negative MR response.[23] Inspired by these works, we made a change on both current flowing direction and magnitude to examine whether negative MR feature can still be kept. As illustrated in Figure 1e, alternation on current size and direction indeed aroused a bit fluctuation on MR size. Even so, primitive negative MR property was well preserved. Migrating to MR loops as shown in Figure 1f, we found MR shape almost stayed unchanged against current variation though MR ratio reduced a bit under increasing current size. With these results, we believe the above negative OSV signal is absolutely not coincident, instead, is the inherent spin response of polymer spin valve thus deserves further exploration.

Like many other reports, we initially questioned whether spin injecting or detecting interface was negatively polarized thus led to such negative MR response. Spin polarization of both bottom NiFe/Au and top PNVT-CN-8/Co interfaces were measured (Figure S5, Supporting Information). Clearly, no negative polarization was found. Therefore, concept of electrode's negative polarization does not fit for explaining our negative MR phenomena. Nonetheless, we cannot ignore the possible influence of TAMR effect on negative MR response, which can even be detected in one FM electrode-left fake valve structure.[56–60] Just recently, Ding discovered the MR signal of NiFe-based

polymer spin valves was rather sensitive to magnetic anisotropy of bottom NiFe injecting electrode.[60] Considering this point, we first checked whether negative MR response can be obtained in TAMR-like devices with the configuration structure of NiFe (bottom)/Au/PNVT-CN-8/Au and Au/PNVT-CN-8/Co (top)/Au. TAMR signal of the former NiFe-based structure is depicted in Figure S6a–c, Supporting Information. Admittedly, MR shape varies with the change on the angle of the in-plane magnetic field relative to the easy axis of the NiFe electrode. In spite of so, TAMR signal of the NiFe/Au/OSC/Au is absolutely positive without negative background peaks. Similar phenomenon was also observed in Au/OSC/Co structure though effective TAMR response aroused until testing current exceeded 10 µA (Figure S6d–f, Supporting Information). Subsequently, we examined if the MR signals of the entire NiFe-based OSV devices inverse as the angle changes from 0° to 90° as diagrammed in **Figure 2**a.[56,57,60] We measured MR loops of the OSV devices possessing the configuration structure of NiFe (bottom)/Au/PNVT-CN-8 (25 nm)/Co (top)/Au at different angles of in-plane magnetic field (Figure 2b). The MR response of the complete OSV device is still negative and does not confront dramatic change on its shape when angle differs between 45° and 90° . Moreover, the MR size reaches its maximum at 45° and that is why we choose such angle for standard MR test. However, when the testing angle decreases from 45° to 0°, both widths and peaks of MR curves change fiercely as illustrated in Figure S7, Supporting Information. Even so, MR response is still negative namely resistance under designed antiparallel state is lower than that measured in parallel state. These results demonstrated the negative OSV effect was not contributed by the TAMR effect arising from the FM electrodes. Recently, Lueso observed MR signal reversal in vertical OSV just by reversing relative position of two FM electrodes NiFe and Co. They attributed this result to the chemical hybridization near OSC/FM interface.[61] As mentioned above, such phenomenon can be classified into spinterface issue, which has been considered as one important negative MR resource since 2010.[18–22] Inspired by this point, we exchanged the original sequence of NiFe and Co electrodes and fabricated control junction arranged as Co (bottom)/Au/PNVT-CN-8/NiFe (top)/Au. Amazingly, such spin polarizer reversal did not change the negative MR effect in standard NiFe (bottom)/Au/PNVT-CN-8/Co (top)/Au sample too much both in size and signal including temperature dependence (Figure S8, Supporting Information). Hence we believed discussing negative MR response also did not arise from specific chemical hybridization near either PNVT-CN-8/NiFe or PNVT-CN-8/Co interface.

Taking a summary of above results, we find this intriguing negative OSV signal is governed by spin dynamics inside the PNVT-CN-8 interlayer. The most effective way to verify this inference is changing thin film states of PNVT-CN-8 spacer and checking whether the negative MR effect can be reproduced. Such idea was extracted from recent theoretical study performed by Schott, which emphasized the importance of processing methods to spin dynamics inside D–A type conjugated polymers.[45] In polymer thin film transistors, the processing solvent has a decisive controlling effect on the film quality and device electronic performance.[62] Similar relationship in polymer spintronics studies have also been
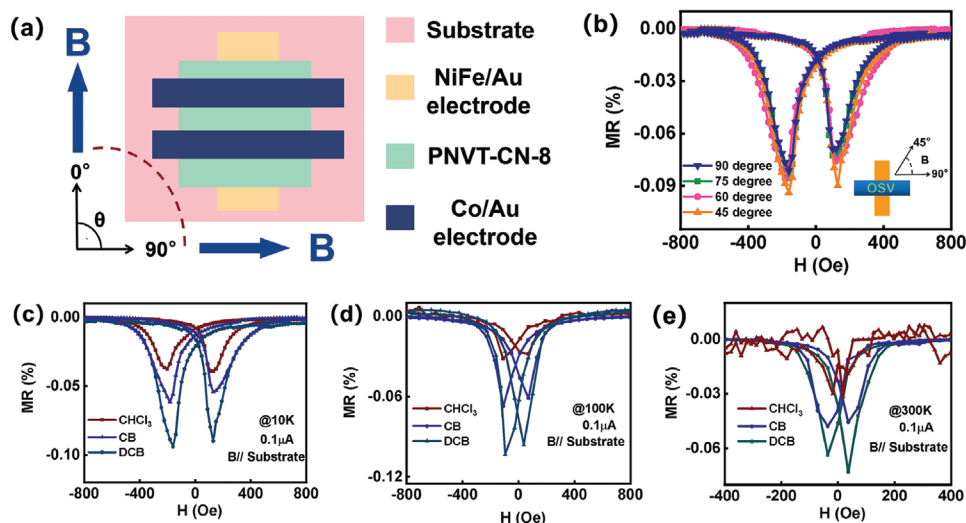
**ADVANCED
SCIENCE NEWS**

www.advancedsciencenews.com

**ADVANCED
MATERIALS
INTERFACES**

www.advmatinterfaces.de

Figure 2. The OSV devices with the configuration structure of NiFe (bottom)/Au/PNVT-CN-8 (25 nm)/Co (top)/Au. a) Diagram of angle sensitivity of complete OSV ranging from 0° to 90°. b) MR loops of the OSV devices measured at different angles (from 90° to 45°) of in-plane magnetic field at 10 K. c–e) MR loops of the OSV devices fabricated by using different solvents measured at temperatures of c) 10, d) 100, and e) 300 K.

predicted and discovered.[63,64] Whereas, research on the interaction between processing solvent selection and OSV performance is still vacant. In our previous OFET-themed article, the polymer PNVT-CN-8 was demonstrated to show good solubility in different solvents. Allowing for this fact, we fabricated another two OSV devices with the configuration structure of NiFe (bottom)/Au/PNVT-CN-8 (25 nm)/Co (top)/Au by using the trichloromethane ($CHCl_3$), and chlorobenzene (CB) solvents to spin-coat the PNVT-CN-8 thin film, respectively. Figure 2c–e shows the MR loops of the corresponding OSV devices fabricated by using $CHCl_3$, CB, and DCB measured at different temperatures. The negative feature of the OSV signal is well preserved regardless of the type of solvents. Furthermore, device fabricated by using the DCB solvent shows the strongest MR negative effect at all temperatures, while the MR response observed for the device fabricated by using $CHCl_3$ is the weakest, merely around –0.03%. Nonetheless, the absolute MR ratios for all three OSV devices have a bearing on the same non-monotonous temperature dependence as illustrated in Figure S9, Supporting Information. Additionally, we also noticed that the MR shape for the device fabricated by using $CHCl_3$ showed more fierce signal-to-noise ratio than those

of the other two devices, especially at room temperature. For better understanding of above MR discrepancy, we characterized the morphology of the PNVT-CN-8 thin film by atomic force microscopy (AFM). Referring to the AFM images listed in **Figure 3**, we found that the surface roughness of the PNVT-CN-8 thin film decreased with the elevation in solvent boiling points. Flatness of the PNVT-CN-8 thin films fabricated by using DCB or CB was controlled below 1 nm. For the polymer films prepared with $CHCl_3$, resulting surface roughness even reached over 2 nm. As repeatedly strengthened by other groups, the morphology of the polymer thin films can impact its spin transport performance significantly.[4,65–67] Enhancing surface roughness of organic transport media can not only reduce the interface quality, but may more seriously increase the possibility of spin scattering, which is not conducive to spin detection. This offers a good explanation to the fact that MR effect for the OSV devices fabricated by using $CHCl_3$ as a solvent is much weaker than that of the other two devices using solvents with higher boiling points. Likewise, the greatest signal/noise fluctuations in MR curve of the OSV devices fabricated by using $CHCl_3$ as a solvent can also be explained by this point. Based on these results, we preliminarily speculate the negative
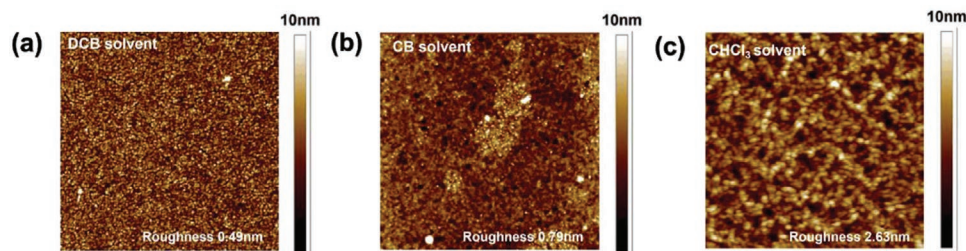

Figure 3. Morphology of the 25 nm PNVT-CN-8 thin film spin-coated by using a) DCB, b) CB, and c) $CHCl_3$. Scan size is 5 μm × 5 μm and data scale is 10 nm. All characterized polymer thin film was grown onto Au surface.

MR effect in the OSV devices based on PNVT-CN-8 relies on spin dynamics inside polymer media.

To better understand the relationship between the negative MR signal and the spin dynamics inside the polymer, we replaced the bottom low-polarization NiFe polarizer into high-polarization perovskite LSMO electrode to fabricate the OSV devices with the configuration structure of LSMO ($La_{07}Sr_{0.3}MnO_3$, bottom)/Au/PNVT-CN-8 (25 nm)/Co (top)/Au (see **Figure 4**a). Compared to the FM metals, half metallic LSMO electrode is more advantageous in spin injection due to its high polarization up to almost 100% at cryogenic temperature, which is much larger than those of FM metals (Co: ≈34%; NiFe: ≈45%).[3,4] In this case, only spin-up polarized states exist in LSMO thin film unlike FM metals according to the spin polarization simulation formula: $(N\uparrow-N\downarrow)/(N\uparrow+N\downarrow) \times 100\%$ ($N\uparrow$ stands for spin-up density, $N\downarrow$ represents spin-down density).[68] From this perspective, analyzing negative MR resource via such half-metal spin polarizer is a better choice. We first measured the MR response of the device fabricated by employing DCB solvent. As shown in Figure 4b, obvious negative MR response

was achieved persisting up to 200 K. Besides, the device resistance decreases with increasing temperature, hence illustrates this LSMO-based polymer spin valve works normally free from short-circuiting. The PNVT-CN-8 thin films spin coated by using CB and $CHCl_3$ solvents also exhibited the negative MR effect (see Figure 4c). Moreover, similar solvent boiling point dependence of the MR loops for the device with the configuration structure of LSMO (bottom)/Au/PNVT-CN-8/Co (top)/Au was also obtained although NiFe electrode was replaced into LSMO thin film, namely the absolute values of negative MR increased with elevation in solvents' boiling point. Temperature dependence of these negative MR signals is displayed in Figure 4d. Apparently, the absolute values of negative MR response for all devices fabricated by using different solvents decreased monotonously with increasing temperature, which can be explained by the low Curie temperature of LSMO electrode itself.[7] It should be noted that all these negative MR responses have nothing to do with LSMO electrode itself or LSMO/Au/Co background structure, as depicted in Figure S10a–c, Supporting Information. Clearly, PNVT-CN-8
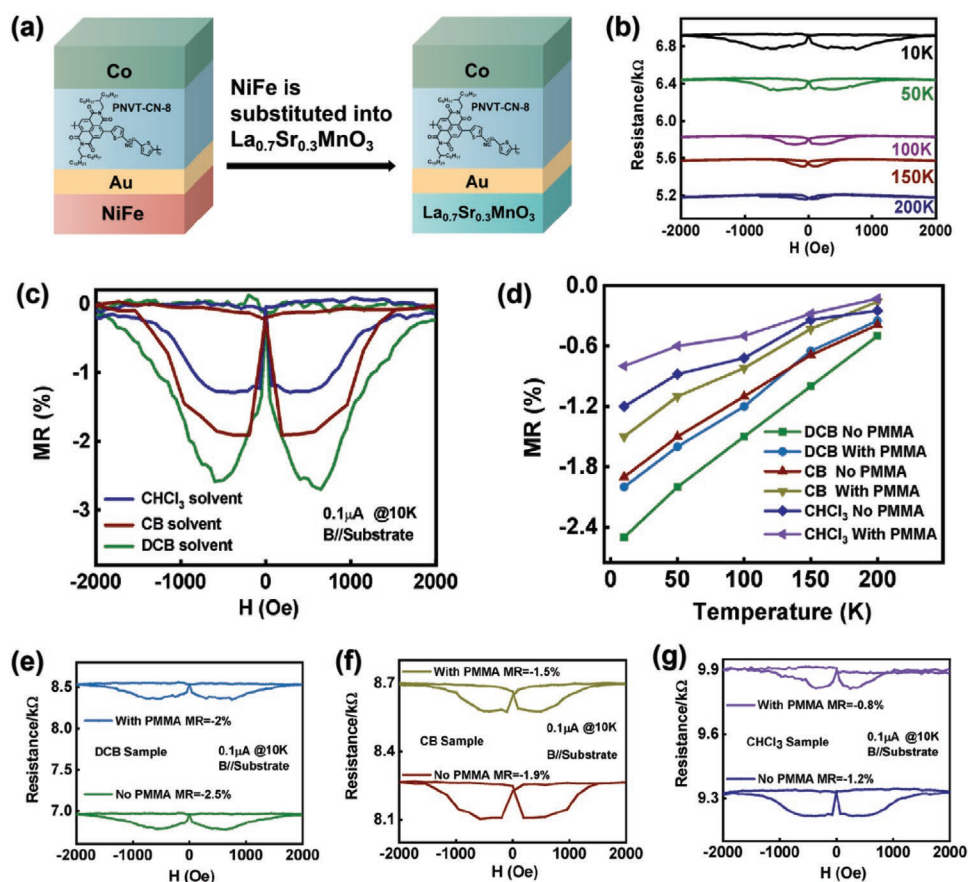

Figure 4. a) Schematic diagram of the OSV devices based on PNVT-CN-8 with a configuration structure of the bottom electrode/Au/PNVT-CN-8/Co (top)/Au. The bottom NiFe electrode was substituted into $La_{0.7}Sr_{0.3}MnO_3$ thin film. b) Device resistance as a function of magnetic field for the LSMO-based OSV devices without the PMMA inserted layer fabricated by using DCB solvent measured at different temperatures. c) MR loops of the LSMO-based OSV devices fabricated without the PMMA inserted layer by using different solvents measured at 10 K. d) MR ratios as a function of temperature for the LSMO-based OSV devices with and without the PMMA inserted layer fabricated by using DCB solvents. e–g) Device resistance as a function of magnetic field for the LSMO-based OSV devices with and without the PMMA inserted layer fabricated by using e) DCB, f) CB, and g) $CHCl_3$ solutions measured at 10 K.

thin film in the above polymer spin valves contacts directly with Co electrode. Though we have already ruled out metal filaments' influence on device conductivity, it is still not enough to ensure that negative MR responses in these LSMO-based spin valves are absolutely free from top metal inclusion and possible reaction at PNVT-CN-8/Co interfaces. To solve this problem, we inserted a 5 nm thin layer of PMMA at PNVT-CN-8/Co interfaces to fabricate another collection of reference devices with a configuration structure of LSMO (bottom)/Au/PNVT-CN-8/PMMA (5 nm)/Co (top)/Au. The PMMA's introduction though has a bit influence on MR size as Figure 4d illustrated, negative MR feature is well kept. In Figure 4e–g, we listed the comparative MR loops of the PNVT-CN-8-based spin valves with and without the PMMA interlayer. Obviously, inserting such kind of buffering barrier neither induces surge on junction resistance nor brings dramatic change on MR shape though negative MR phenomenon is acquired. On the contrary, the background device with a configuration structure of LSMO/Au/PMMA (5 nm)/Co/Au exhibits positive MR response as shown in Figure S10, Supporting Information. Based on these results, we solidly believe spin dynamics inside the D–A polymer layer is the only responsible origin for these negative MR responses.

All polymer spin valves discussed in this work contain a device structure of the bottom electrode/Au/PNVT-CN-8/top electrode, where the bottom and top electrodes were used as spin polarizer and spin collector, respectively. To better comprehend negative MR effect, we selected the LSMO (bottom)/Au/PNVT-CN-8/Co (top) system for further discussion. Since device with the configuration structure of the LSMO/Au/Co exhibited the positive MR response, we believed that injected spin-up polarized carriers did not encounter severe spin orientation reversal when traversing this 3 nm Au interlayer. Corresponding diagram of the spin transport for the LSMO (bottom)/Au/Co (top) is depicted in **Figure 5**a. After introducing PNVT-CN-8 between Au and Co, spin-up polarized carriers from LSMO electrode can encounter reversal on their orientation, and thus become spin-down polarized states as illustrated in Figure 5b. In this case, reversed spin-down carriers are scattered when arriving at the detection electrode whose spin-up

density overwhelms spin-down density. Owing to this point, defined parallel state is actually transformed into antiparallel state and vice versa. The negative MR effect then is acquired as displayed on the right of Figure 5b. Such reversal on spin orientation is similar to spin-filtering phenomenon which is a kind of spin selectivity process.[69–71] Concept of spin filtering was also used for explanation toward reversed MR signals as recently discovered in molecular spin valves exploiting organic radical self-assembled monolayer and 2D materials.[72–76] Since our negative MR response is contributed by bulk spin transport rather than spinterface engineering, we prefer to use "filtering-like" term to define such spin reversal activity of bulk spin transport. This is the first report on such fascinating spin phenomenon in solution-processed conjugated D–A polymers.

Intermolecular interactions between donor and acceptor moieties play important roles in the dynamic property within D–A conjugated polymers, which has been thoroughly and extensively probed in electronics community.[38–41] Similar relationship was also discussed in our group's recent spin transport study concerning D–A conjugated polymers.[11,44] As we just mentioned, filtering-like spin dynamics inside PNVT-CN-8 is the determining reason for the negative OSV signal. Since it is so, examining whether spin orientation reversal inside the D–A conjugated polymers is prone to the strength of intermolecular interactions between donor and acceptor moieties naturally becomes another critical issue. To gain effective contrast, herein we extended the alkyl-chain length on nitrogen atoms of acceptor NDI unit thus obtained polymer PNVT-CN-10 whose structure is shown in Figure S11, Supporting Information. Such alkyl-chain extension was reported to lead to longer d–d distance thus weaker intermolecular interaction in PNVT-CNs polymer by our group previously.[47] Therefore, it is a good strategy to investigate the intermolecular interaction dependence of the spin reversal activity within the conjugated D–A polymers. Before discussing its MR behavior, we want to strengthen PNVT-CN-10 shares the same energy-level distributions with PNVT-CN-8,[47] as a result, interfacial spin injection efficiency in the PNVT-CN-10 devices is also identical to that of the PNVT-CN-8 spin valves. We first investigated PNVT-CN-10's
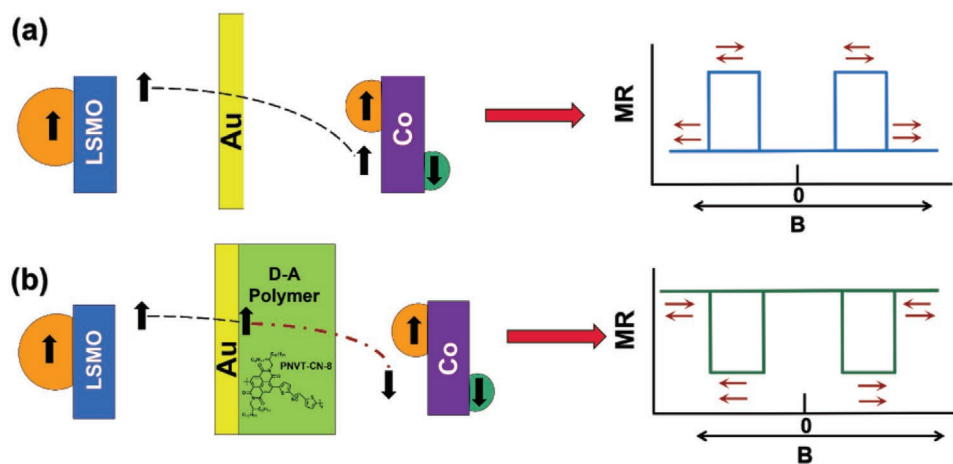

Figure 5. a) Diagram of spin transport and resulting positive MR response of the LSMO/Au/Co spin valve (without PNVT-CN-8 polymer). b) Diagram of spin transport and resulting negative MR response of the LSMO/Au/PNVT-CN-8/Co spin valve.
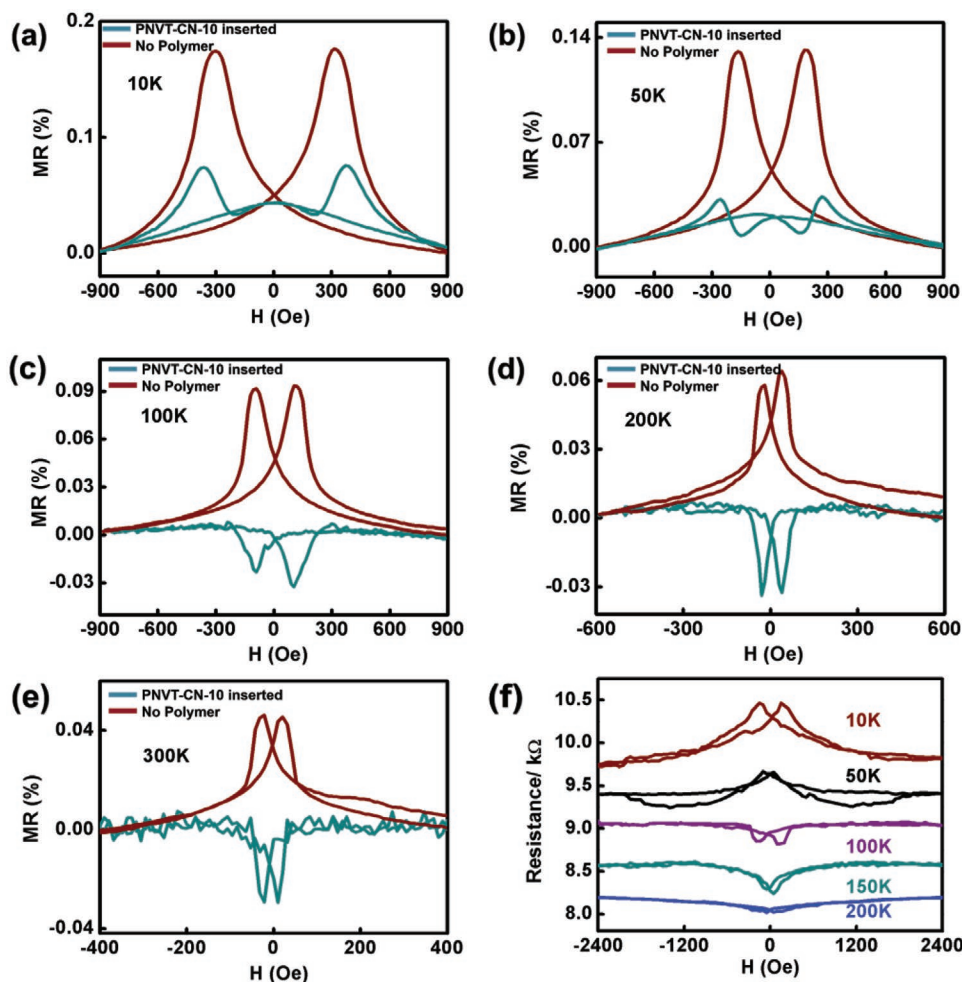
ADVANCED
SCIENCE NEWS
www.advancedsciencenews.com

ADVANCED
MATERIALS
INTERFACES
www.advmatinterfaces.de

Figure 6. a–e) MR loops of the OSV devices with the configuration structure of NiFe (bottom)/Au/PNVT-CN-10 (25 nm)/Co (top)/Au and NiFe (bottom)/Au/Co(top)/Au measured at different temperatures. f) Device resistance as a function of magnetic field for the OSV devices with the configuration structure of LSMO (bottom)/Au/PNVT-CN-10 (25 nm)/Co (top)/Au measured at different temperatures.

MR response in FM-metal polarization networks. Of course, device configuration structure was identical to that of PNVT-CN-8, namely NiFe (12 nm, bottom)/Au (3 nm)/PNVT-CN-10 (25 nm)/Co (12 nm, top)/Au (25 nm) also for effective comparison. Under the same four-probe testing method, MR signal of PNVT-CN-10-based OSV devices was measured and is shown in **Figure 6**a–e. To better manifest polymer's contribution, we showed MR response of in-situ metallic background simultaneously in these figures. Beyond our imagination, measured OSV signals in PNVT-CN-10 junction exhibit temperature-dependent MR sign reversal from 10 to 300 K. Below 100 K, MR response of the OSV devices based on the polymer PNVT-CN-10 with longer alkyl-chains is four-resistive-like state, which contains both positive and negative MR peaks. This indicates the OSV signal is partially contributed by background metallic spin valve which possibly owes to the weaker filtering-like spin dynamics inside PNVT-CN-10. When temperature increases from 100 to 300 K, prototype negative MR response then arises and conceals the positive MR contribution from background metallic structure. Compared to PNVT-CN-8-based

OSV devices using the same FM-metal polarizers, negative OSV signal in this PNVT-CN-10-based device is much weaker whose room temperature MR value is just around −0.3%. Based on this point, we conclude that the possibility of spin-orientation reversal is in positive proportion to the strength of intermolecular interaction within D–A polymers. Similar temperature-dependent MR signal transition was achieved in LSMO (La$_{07}$Sr$_{0.3}$MnO$_3$, bottom)/Au/PNVT-CN-10 (25 nm)/Co (top)/Au structure as illustrated in Figure 6f. These results further demonstrated investigating spin dynamics inside D–A polymer should better be associated with molecular engineering project.

3. Conclusion

We utilize the D–A type conjugated polymer based on NDI and 2,3-bis(thiophen-2-yl) acrylonitrile units as the spacer to fabricate the OSV devices with configuration structure of NiFe (12 nm)/Au (3 nm)/PNVT-CN-8 (25 nm)/Co (12 nm)/Au (25 nm). The negative MR effect was observed at temperature

**ADVANCED
SCIENCE NEWS**
www.advancedsciencenews.com

**ADVANCED
MATERIALS
INTERFACES**
www.advmatinterfaces.de

ranging from 10 to 300 K. This is entirely opposite to underlying all-metal background NiFe/Au (3 nm)/Co/Au structure whose MR response is absolute positive. Besides, this interesting negative MR behavior is well repeatable against current variation and air exposure. We also clarified that the resulting negative MR signal arises from neither angle-dependent anisotropy of complete OSV nor TAMR effect in underlying single FM-electrode contained fake valve structure. The negative MR signal was also achieved in the OSV devices with the configuration structure of Co (bottom, 12 nm)/Au (3 nm)/PNVT-CN-8 (25 nm)/NiFe (top, 12 nm)/Au (25 nm). This experimental result further demonstrates the negative MR nature is not decided by specific hybridization between PNVT-CN-8 and FM metals. The above results give solid support to the governing role of polymer PNVT-CN-8 itself on the negative MR phenomenon. To figure out the origin of the negative MR effect, we finally substituted the bottom FM metal electrode into high-polarization LSMO thin film for further discussion. Under the device arranged as LSMO (bottom)/Au/PNVT-CN-8 (25 nm)/Co (top)/Au, negative MR behavior was reproduced and also exhibited similar dependence up to 200 K. To ensure measured negative MR signals are not affected by metal/organic interpenetration or chemical reaction at PNVT-CN-8/Co interfaces, we inserted a 5 nm PMMA layer at top PNVT-CN-8/Co interfaces. Fortunately, the inserted PMMA buffering layer did not remove the negative MR feature though had a bit influence on the MR ratios. These results powerfully demonstrate that the negative MR effect is solely determined by spin dynamics inside PNVT-CN-8 thin film. We hold the spin-orientation reversal inside D–A polymer spacer is the ultimate explanation to the negative MR response. Furthermore, such filtering-like spin activity is dependent on intermolecular interaction between donor and acceptor units according to the MR discrepancy between PNVT-CN-8 and PNVT-CN-10. This work proposes a novel perspective to comprehend spin transport phenomenon in solution-processed D–A polymers, also paves a new way to manipulate spin by molecules.

4. Experimental Section

Preparation of the NDI-Based Conjugated Polymer: Synthetic details can be found in a previous OFET-themed article.[47]

Fabrication of the NiFe (Bottom)/Au/PNVT-CN-8 (25 nm)/Co (Top)/Au Device: The Si/SiO$_2$ substrate was selected for the construction of the OSVs. This substrate was ultrasonically cleaned before depositing ferromagnetic electrode. Cleaning sequence was as follows: 1) Ultrasonication by de-ionized water for 5 min, and then transferred to the oven for drying; 2) Ethanol ultrasonication for 5 min, and then dried in oven; 3) Acetone ultrasonic cleaning for 5 min, and then dried and performed ultraviolet ozone treatment for 20 min. After finishing these steps, these substrates were transferred into the glove box filled with nitrogen and then covered them with the strip-shaped shadow mask before placing them into the vacuum evaporation chamber. When the vacuum was evacuated to 5×10^{-4} Pa, a 5 nm Au thin film was first deposited as the adhesion layer of the bottom ferromagnetic electrode. After that, the NiFe electrode deposition was started without breaking the vacuum until the chamber inner pressure reached 2×10^{-4} Pa. The evaporation process was divided into two steps with various evaporation rates. At the stage of the first 3 nm, the evaporation rate was set as 0.1 Å s^{-1}. As for the remaining 9 nm (target thickness was 12 nm), the evaporation rate was controlled within a range of 0.5–0.6 Å s^{-1}.

After completing the NiFe electrode deposition, then the 3 nm Au thin film was evaporated as a protective layer onto the NiFe thin film without breaking the vacuum. Afterward, these substrates capped with NiFe electrodes were transferred into glove-box to perform polymer thin film deposition. The PNVT-CN-8 thin film was spin-coated onto the NiFe/Au thin films. In order to remove the residual solvent from the organic film, the polymer covered substrate was placed onto the hot plate inside the glove box to undertake annealing treatment. After finishing polymer thin films preparation, shadow mask was capped on top of them to fabricate a Co top electrode. For the Co top electrode, depositing method was similar to the bottom NiFe electrode. Two-step deposition method was used for electrode fabrication. The first 5 nm thin film was finished at the evaporation rate of 0.1 Å s^{-1}. The remaining 7 nm Co thin film was completed at the evaporation rate of 0.5–0.6 Å s^{-1}. At last, 25 nm Au thin film was covered adjacent to Co electrode for void of oxidation.

Fabrication of the Co (Bottom)/Au/PNVT-CN-8 (25 nm)/NiFe (Top)/Au Device: Compared to the NiFe (bottom)/Au/PNVT-CN-8 (25 nm)/Co (top)/Au, just NiFe and Co sequence was reversed. Corresponding deposition parameters were identical to those in the NiFe (bottom)/Au/PNVT-CN-8/Co (top)/Au structure.

Fabrication of the NiFe (Bottom)/Au/PNVT-CN-8 (15 nm)/Co (Top)/Au Device: In contrast to the NiFe (bottom)/Au/PNVT-CN-8 (25 nm)/Co (top)/Au device, only the thickness of PNVT-CN-8 thin film was changed from 25 to 15 nm while keep the other sections identical to that of standard NiFe (bottom)/Au/PNVT-CN-8 (25 nm)/Co (top)/Au device.

Fabrication of the NiFe (Bottom)/Au/PNVT-CN-10 (25 nm)/Co (Top)/Au Device: The only difference on device fabrication compared to the NiFe (bottom)/Au/PNVT-CN-8 (25 nm)/Co (top)/Au junction was the polymer spacer was substituted into PNVT-CN-10 which was dissolved by DCB solvent.

Fabrication of the LSMO (Bottom)/Au/PNVT-CN-8 (25 nm)/Co (Top)/Au Device: The LSMO film as the bottom electrode was fabricated by a pulsed laser deposition method on SrTiO$_3$ substrates and then etched to strip pattern by an ion beam etching process. As for other sections, the related fabrication methods and parameters of the PNVT-CN-8 spacer and the top Co electrode were identical to those in NiFe (bottom)/Au/PNVT-CN-8 (25 nm)/Co (top)/Au structure.

Fabrication of the LSMO (Bottom)/Au/PNVT-CN-10 (25 nm)/Co (Top)/Au Device: Just the interlayer polymer of LSMO (bottom)/Au/PNVT-CN-8 (25 nm)/Co (top)/Au was changed from PNVT-CN-8 to PNVT-CN-10 while keeping other components prepared identically to that of LSMO (bottom)/Au/PNVT-CN-8 (25 nm)/Co (top)/Au.

MR Measurement Methods: All MR signals were measured by the physical property measurement system. As for the measurement about magnetic hysteresis loops of ferromagnetic electrodes, vibrating sample magneto-meter was employed.

Supporting Information

Supporting Information is available from the Wiley Online Library or from the author.

Conflict of Interest

The authors declare no conflict of interest.

[1] V. A. Dediu, L. E. Hueso, I. Bergenti, C. Taliani, *Nat. Mater.* **2009**, *8*, 707.

[2] D. Sun, E. Ehrenfreund, Z. V. Vardeny, *Chem. Commun.* **2014**, *50*, 1781.

[3] J. Devkota, R. Geng, R. C. Subedi, T. D. Nguyen, *Adv. Funct. Mater.* **2016**, *26*, 3881.

[4] H. J. Jang, C. A. Richter, *Adv. Mater.* **2017**, *29*, 1607239.

[5] L. Guo, X. Gu, X. Zhu, X. Sun, *Adv. Mater.* **2019**, *31*, 1805355.

[6] J. Tsurumi, H. Matsui, T. Kubo, R. Hausermann, C. Mitsui, T. Okamoto, S. Watanabe, J. Takeya, *Nat. Phys.* **2017**, *13*, 994.

[7] Z. H. Xiong, D. Wu, Z. Valy Vardeny, J. Shi, *Nature* **2004**, *427*, 821.

[8] A. R. Rocha, V. M. García-Suarez, S. W. Bailey, C. J. Lambert, J. Ferrer, S. Sanvito, *Nat. Mater.* **2005**, *4*, 335.

[9] D. Sun, L. Yin, C. Sun, H. Guo, Z. Gai, X. G. Zhang, T. Z. Ward, Z. Cheng, J. Shen, *Phys. Rev. Lett.* **2010**, *104*, 236602.

[10] S. Ding, Y. Tian, H. Wang, Z. Zhou, W. Mi, Z. Ni, Y. Zou, H. Dong, H. Gao, D. Zhu, W. Hu, *ACS Nano* **2018**, *12*, 12657.

[11] Y. Zheng, Y. Feng, D. Gao, N. Zheng, D. Li, L. Jiang, X. Wang, K. Jin, G. Yu, *Adv. Electron. Mater.* **2019**, *5*, 1900318.

[12] J. Wang, C. Zhang, H. Liu, R. McLaughlin, Y. Zhai, S. R. Vardeny, X. Liu, S. McGill, D. Semenov, H. Guo, R. Tsuchikawa, V. V. Deshpande, D. Sun, Z. V. Vardeny, *Nat. Commun.* **2019**, *10*, 129.

[13] W. Yang, Q. Shi, T. Miao, Q. Li, P. Cai, H. Liu, H. Lin, Y. Bai, Y. Zhu, Y. Yu, L. Deng, W. Wang, L. Yin, D. Sun, X. Zhang, J. Shen, *Nat. Commun.* **2019**, *10*, 3877.

[14] X. Song, X. Wang, Y. Li, C. Zheng, B. Zhang, C.-a. Di, F. Li, C. Jin, W. Mi, L. Chen, W. Hu, *Angew. Chem., Int. Ed.* **2020**, *599*, 1118.

[15] M. Julliere, *Phys. Lett. A* **1975**, *54*, 225

[16] J. M. De Teresa, A. Barthelemy, A. Fert, J. P. Contour, F. Montaigne, P. Seneor, *Science* **1999**, *286*, 507.

[17] S. Mandal, R. Pati, *ACS Nano* **2012**, *6*, 358.

[18] S. Sanvito, *Nat. Phys.* **2010**, *6*, 562.

[19] M. Cinchetti, V. A. Dediu, L. E. Hueso, *Nat. Mater.* **2017**, *16*, 507.

[20] C. Barraud, P. Seneor, R. Mattana, S. Fusil, K. Bouzehouane, C. Deranlot, P. Graziosi, L. Hueso, I. Bergenti, V. Dediu, F. Petroff, A. Fert, *Nat. Phys.* **2010**, *6*, 615.

[21] D. Ciudad, M. Gobbi, C. J. Kinane, M. Eich, J. S. Moodera, L. E. Hueso, *Adv. Mater.* **2014**, *26*, 7561.

[22] S. Ding, Y. Tian, Y. Li, W. Mi, H. Dong, X. Zhang, W. Hu, D. Zhu, *ACS Appl. Mater. Interfaces* **2017**, *9*, 15644.

[23] H. Vinzelberg, J. Schumann, D. Elefant, R. B. Gangineni, J. Thomas, B. Buchner, *J. Appl. Phys.* **2008**, *103*, 093720.

[24] M. Prezioso, A. Riminucci, I. Bergenti, P. Graziosi, D. Brunel, V. A. Dediu, *Adv. Mater.* **2011**, *23*, 1371.

[25] R. Göckeritz, N. Homonnay, A. Müller, T. Richter, B. Fuhrmann, G. Schmidt, *Appl. Phys. Lett.* **2015**, *106*, 102403.

[26] R. Göckeritz, N. Homonnay, A. Müller, B. Fuhrmann, G. Schmidt, *AIP Adv.* **2016**, *6*, 045003.

[27] Z. Wen, D. Wu, *Adv. Mater.* **2019**, *31*, 1904123.

[28] X. Zhang, J. Tong, H. Zhu, Z. Wang, L. Zhou, S. Wang, T. Miyashita, M. Mitsuishi, G. Qin, *J. Mater. Chem. C* **2017**, *5*, 5055.

[29] D. Pantel, S. Goetze, D. Hesse, D. M. Alexe, *Nat. Mater.* **2012**, *11*, 289.

[30] V. Garcia, M. Bibes, *Nat. Commun.* **2014**, *5*, 4289.

[31] S. Liang, H. Yang, H. Yang, B. Tao, A. Djeffal, M. Chshiev, W. Huang, X. Li, A. Ferri, R. Desfeux, S. Mangin, D. Lacour, M. Hehn, O. Copie, K. Dumesnil, Y. Lu, *Adv. Mater.* **2016**, *28*, 10204.

[32] G. Lu, J. Blakesley, S. Himmelberger, P. Pingel, J. Frisch, I. Lieberwirth, I. Salzmann, M. Oehzelt, R. Di Pietro, A. Salleo, N. Koch, D. Neher, *Nat. Commun.* **2013**, *4*, 1588.

[33] B. Lüssem, C.-M. Keum, D. Kasemann, B. Naab, Z. Bao, K. Leo, *Chem. Rev.* **2016**, *116*, 13714.

[34] Z. G. Yu, *Nat. Commun.* **2014**, *5*, 4842.

[35] I. Bergenti, F. Borgatti, M. Calbucci, A. Riminucci, R. Alberto Cecchini, P. Graziosi, D. MacLaren, A. Giglia, J. P. Rueff, D. Ceolin, L. Pasquali, V. Dediu, *ACS Appl. Mater. Interfaces* **2018**, *10*, 8132.

[36] A. Riminucci, Z.-G. Yu, M. Prezioso, R. Cecchini, I. Bergenti, P. Graziosi, V. A. Dediu, *ACS Appl. Mater. Interfaces* **2019**, *11*, 8319.

[37] D. Sun, Y. Zhai, K. van Schooten, C. Zhang, M. Kavand, H. Malissa, M. Groesbeck, R. Menon, C. Boehme, Z. Vardeny, *J. Phys.: Condens. Matter* **2018**, *30*, 484003.

[38] H. Chen, Y. Guo, G. Yu, Y. Zhao, J. Zhang, D. Gao, H. Liu, Y. Liu, *Adv. Mater.* **2012**, *24*, 4618.

[39] K. Shi, W. Zhang, D. Gao, S. Zhang, Z. Lin, Y. Zou, L. Wang, G. Yu, *Adv. Mater.* **2018**, *30*, 1705286.

[40] Y. Ren, X. Yang, L. Zhou, J. Mao, S. Han, Y. Zhou, *Adv. Funct. Mater.* **2019**, *29*, 1902105.

[41] G. J. Hedley, A. Ruseckas, I. D. Samuel, *Chem. Rev.* **2017**, *117*, 796.

[42] F. Li, T. Li, F. Chen, F. Zhang, *Sci. Rep.* **2015**, *5*, 9355.

[43] G. Q. Zhou, G. Tang, T. Li, G. Pan, Z. Deng, F. Zhang, *J. Phys. D: Appl. Phys.* **2017**, *50*, 095001.

[44] D. Li, X. Wang, Z. Lin, Y. Zheng, Q. Jiang, N. Zheng, W. Zhang, K. Jin, G. Yu, *ACS Appl. Mater. Interfaces* **2019**, *11*, 30089.

[45] S. Schott, U. Chopra, V. Lemaur, A. Melnyk, Y. Olivier, R. Di Pietro, I. Romanov, R. L. Carey, X. Jiao, C. Jellett, M. Little, A. Marks, C. R. McNeill, I. McCulloch, E. R. McNellis, D. Andrienko, D. Beljonne, J. Sinova, H. Sirringhaus, *Nat. Phys.* **2019**, *15*, 814.

[46] N. Zheng, Z. Lin, Y. Zheng, D. Li, J. Yang, W. Zhang, L. Wang, G. Yu, *Org. Electron.* **2020**, *81*, 105684.

[47] Z. Lin, X. Liu, W. Zhang, C. Wei, J. Huang, Z. Chen, L. Wang, G. Yu, *J. Polym. Sci., Part A: Polym. Chem.* **2017**, *55*, 3627.

[48] H. Chen, Y. Guo, Z. Mao, G. Yu, J. Huang, Y. Zhao, Y. Liu, *Chem. Mater.* **2013**, *25*, 3589.

[49] G. Schmidt, D. Ferrand, L. Molenkamp, A. Filip, B. van Wees, *Phys. Rev. B* **2000**, *62*, R4790.

[50] S. Mooser, J. F. K. Cooper, K. K. Banger, J. Wunderlich, H. Sirringhaus, *Phys. Rev. B: Condens. Matter Mater. Phys.* **2012**, *85*, 235202.

[51] S.-J. Wang, D. Venkateshvaran, M. R. Mahani, U. Chopra, E. R. McNellis, R. Di Pietro, S. Schott, A. Wittmann, G. Schweicher, M. Cubukcu, K. Kang, R. Carey, T. J. Wagner, J. N. M. Siebrecht, D. P. G. H. Wong, I. E. Jacobs, R. O. Aboljadayel, A. Ionescus, S. A. Egorov, S. Mueller, O. Zadvorna, P. Skalski, C. Jellett, M. Little, A. Marks, I. McCulloch, J. Wunderlich, J. Sinova, H. Sirringhaus, *Nat. Electron.* **2019**, *2*, 98.

[52] X. Sun, M. Gobbi, A. Bedoya-Pinto, O. Txoperena, F. Golmar, R. Llopis, A. Chuvilin, F. Casanova, L. E. Hueso, *Nat. Commun.* **2013**, *4*, 2794.

[53] T. L. A. Tran, T. Q. Le, J. G. M. Sanderink, W. G. van der Wiel, M. P. de Jong, *Adv. Funct. Mater.* **2012**, *22*, 1180.

[54] J.-W. Yoo, H. W. Jang, V. N. Prigodin, C. Kao, C. B. Eom, A. J. Epstein, *Synth. Met.* **2010**, *160*, 216.

[55] S. W. Jiang, B. B. Chen, P. Wang, Y. Zhou, Y. J. Shi, F. J. Yue, H. F. Ding, D. Wu, *Appl. Phys. Lett.* **2014**, *104*, 262402.

[56] T. S. Plaskett, P. P. Freitas, N. P. Barradas, M. F. Da Silva, J. C. Soares, *J. Appl. Phys.* **1994**, *76*, 6104.

[57] T. Kamiya, C. Miyahara, H. Tada, *Appl. Phys. Lett.* **2017**, *110*, 032401.

[58] K. Wang, J. G. M. Sanderink, T. Bolhuis, W. G. van der Wiel, M. P. de Jong, *Phys. Rev. B: Condens. Matter Mater. Phys.* **2014**, *89*, 174419.

[59] K. Wang, E. Strambini, J. G. M. Sanderink, T. Bolhuis, W. G. van der Wiel, M. P. de Jong, *ACS Appl. Mater. Interfaces* **2016**, *8*, 28349.

[60] S. Ding, Y. Tian, H. Dong, D. Zhu, W. Hu, *ACS Appl. Mater. Interfaces* **2019**, *11*, 11654.

[61] A. Bedoya-Pinto, S. G. Miralles, S. Velez, A. Atxabal, P. Gargiani, M. Valvidares, F. Casanova, E. Coronado, L. E. Hueso, *Adv. Funct. Mater.* **2018**, *28*, 1702099.

[62] B. H. Sirringhaus, *Adv. Mater.* **2005**, *17*, 2411.

[63] Z. G. Yu, F. Ding, H. Wang, *Phys. Rev. B* **2013**, *87*, 205446.

[64] N. A. Morley, H. R. H. AlQahtani, M. P. Hodges, M. R. J. Gibbs, M. Grell, V. Dediu, D. J. Morgan, *Appl. Surf. Sci.* **2013**, *265*, 570.

[65] T. D. Nguyen, F. Wang, X.-G. Li, E. Ehrenfreund, Z. V. Vardeny, *Phys. Rev. B* **2013**, *87*, 075205.

[66] X. Zhang, Q. Ma, K. Suzuki, A. Sugihara, G. Qin, T. Miyazaki, S. Mizukami, *ACS Appl. Mater. Interfaces* **2015**, *7*, 4685.

[67] X. Sun, A. Bedoya-Pinto, Z. Mao, M. Gobbi, W. Yan, Y. Guo, A. Atxabal, R. Llopis, G. Yu, Y. Liu, A. Chuvilin, F. Casanova, L. E. Hueso, *Adv. Mater.* **2016**, *28*, 2609.

[68] T. Arnold, A. Atxabal, S. Parui, L. E. Hueso, *Adv. Funct. Mater.* **2018**, *28*, 1706105.

[69] S. Lach, A. Altenhof, K. Tarafder, F. Schmitt, M. E. Ali, M. Vogel, J. Sauther, P. M. Oppeneer, C. Ziegler, *Adv. Funct. Mater.* **2012**, *22*, 989.

[70] K. M. Alam, S. Pramanik, *Adv. Funct. Mater.* **2015**, *25*, 3210

[71] T. Song, X. Cai, M. W.-Y. Tu, X. Zhang, B. Huang, N. P. Wilson, K. L. Seyler, L. Zhu, T. Taniguchi, K. Watanabe, M. A. McGuire, D. H. Cobden, D. Xiao, W. Yao, X. Xu, *Science* **2018**, *360*, 1214.

[72] L. Poggini, G. Cucinotta, A.-M. Pradipto, M. Scarrozza, P. Barone, A. Caneschi, P. Graziosi, M. Calbucci, R. Cecchini, V. A. Dediu, S. Picozzi, M. Mannini, R. Sessoli, *Adv. Mater. Interfaces* **2016**, *3*, 1500855.

[73] A. K. Singh, J. Eom, *ACS Appl. Mater. Interfaces* **2014**, *6*, 2493.

[74] M. Gurram, S. Omar, B. J. van Wees, *2D Mater* **2018**, *5*, 032004.

[75] M. Z. Iqbal, S. Siddique, G. Hussain, *Adv. Eng. Mater.* **2018**, *20*, 1700692.

[76] M. V. Kamalakar, A. Dankert, P. J. Kelly, S. P. Dash, *Sci. Rep.* **2016**, *6*, 21168.